Effect of growth rate and pH on lithium incorporation in calcite

A. Füger [a,b], F. Konrad [a,c], A. Leis [b], M. Dietzel [a], V. Mavromatis [a,d,*]

[a] *Institute of Applied Geosciences, Graz University of Technology, Rechbauerstrasse 12, 8010 Graz, Austria*
[b] *JR-AquaConSol GmbH, Steyrergasse 21, 8010 Graz, Austria*
[c] *Omya GmbH, Gersheim Straße 1-2, 9722 Gummern, Austria*
[d] *Géosciences Environnement Toulouse (GET), CNRS, UMR 5563, Observatoire Midi-Pyrénées, 14 Avenue Edouard Belin, 31400 Toulouse, France*

Abstract

Carbonates are only a minor sink of oceanic lithium, yet the presence of this element and its abundance relative to other metal cations in natural carbonate minerals is routinely used as a paleo-environmental proxy. To date, however, experimental studies on the influence of physicochemical parameters that may control lithium incorporation in calcite, like pH and precipitation rate, are scarce. Therefore, we experimentally studied Li incorporation in calcite to quantify the apparent partitioning coefficient ($D_{Li}^* = \frac{(c_{Li}/c_{Ca})_{calcite}}{(m_{Li^+}/m_{Ca^{2+}})_{solution}}$) between calcite and reactive fluid as a function of calcite growth rate and pH. The obtained results suggest that D_{Li}^* increases with calcite growth rate, according to the expression:

$$\text{Log}D_{Li}^* = 1.331(\pm 0.116) \times \text{Log}Rate + 6.371(\pm 0.880) \quad (\text{R}^2 = 0.87; 10^{-8.1} \leq Rate \leq 10^{-7.1} \text{ mol m}^{-2} \text{ s}^{-1})$$

Additionally the experimental results suggest that D_{Li}^* values exhibit a strong pH dependence. For experiments conducted at similar growth rates (i.e. $Rate = 10^{-7.7\pm0.2}$ mol m^{-2} s^{-1}), D_{Li}^* decreases with increasing pH as described by:

$$\text{Log}D_{Li}^* = -0.57(\pm 0.047) \times \text{pH} + 0.759(\pm 0.366) \quad (\text{R}^2 = 0.90; 6.3 < pH < 9.5)$$

The positive correlation of D_{Li}^* with calcite growth rate is consistent with an increasing entrapment of traces/impurities at rapidly growing calcite surfaces, although the incorporation of monovalent cations such as Li$^+$ and Na$^+$ does not necessarily imply a substitution of Ca^{2+} ions in the calcite crystal lattice. The dependence of D_{Li}^* on pH can be considered as an indication that activity of aqueous HCO$_3^-$ controls the incorporation of Li$^+$ in calcite. The proposed coupled reaction can be explained by charge balance of these monovalent species, which is likely valid at least during the initial step of adsorption on the crystal surface. These new findings shed light on the mechanisms controlling Li incorporation in calcite and have direct implications on the use of Li partitioning coefficients in natural carbonates as an environmental proxy.

* Corresponding author at: Institute of Applied Geosciences, Graz University of Technology, Rechbauerstrasse 12, 8010 Graz, Austria.
E-mail address: mavromatis@tugraz.at (V. Mavromatis).

1. INTRODUCTION

1.1. General background

The trace elemental and isotopic composition of natural carbonate minerals is routinely used by the geoscientific community in order to elucidate the environmental conditions that occurred during mineral formation. In this regard, the mechanisms controlling chemical and isotopic fractionation during $CaCO_3$ mineral formation have been the subject of numerous experimental studies over the last four decades (e.g. Lorens, 1981; Mucci and Morse, 1983; Busenberg and Plummer, 1985; Mucci, 1988; Dromgoole and Walter, 1990; Dietzel and Usdowski, 1996; Tesoriero and Pankow, 1996; Boettcher, 1998; Dietzel et al., 2004; Lakshtanov and Stipp; 2004; 2007; Gabitov and Watson, 2006; Tang et al., 2008a; 2008b; Mavromatis et al., 2013; 2015; 2017a; 2018; Gabitov et al., 2014a; 2014b; Purgstaller et al., 2016; 2017; Voigt et al., 2017). The incorporation of trace elements in carbonate minerals, however, is not controlled only by physicochemical parameters such as temperature, pH and solution composition. It is also affected by the chemical properties of each element and by the crystal structure of the forming mineral phase. For example, spectroscopic techniques have revealed that the incorporation of divalent cations in calcite and aragonite has been shown to follow an ideal substitution of the Ca^{2+} ion in the crystal lattice (e.g. Reeder et al., 1999). This mechanism is not valid for monovalent or trivalent cations, however, due to ionic radii differences and the charge imbalance that is provoked by such substitution.

In the present study, we investigate the mechanisms controlling the incorporation of lithium ion (Li^+) in calcite. We experimentally study the incorporation behavior of Li^+ as a function of calcite growth rate and pH of the forming fluid. While lithium is readily incorporated into biotite, cordierite, alkali-feldspar, spodumene and petalite, it exhibits low concentrations in carbonate minerals of both biogenic and abiotic origin (Burton and Vigier, 2011). As such, the major source of Li in oceanic waters mainly originates from the weathering of continental silicate rocks and its transport via rivers and groundwaters (e.g. Chan et al., 1992; Huh et al., 2001; Négrel et al., 2010). Once introduced into the oceans, major sinks of Li can be ascribed to sea-floor alteration and partly to incorporation into marine carbonates (Misra and Froelich, 2012). Note here that Li is a strongly hydrophilic element that does not readily form aquocomplexes. Moreover, lithium is not utilized in biological systems, thus Li/Ca ratios of marine carbonates have the potential to provide information about changes of global environmental conditions like continental weathering, marine hydrothermal activity, sea level and temperature (Misra and Froelich, 2012). Actually the Li content of marine calcites, and more routinely its ratio to major or trace elements in biomineral exoskeletons (i.e. Li/Ca, Li/Mg, Li/Sr), is used to infer physicochemical parameters of forming natural solutions such as dissolved inorganic carbon and/or degree of seawater saturation with respect to calcite (Hall and Chan, 2004; Lear and Rosenthal, 2006; Lear et al., 2010; Vigier et al., 2015), temperature (Hall and Chan, 2004; Marriott et al., 2004a; Bryan and Marchitto, 2008; Lear et al., 2010), and growth rate (Hall and Chan, 2004). To date however, information about the impact of physicochemical conditions on the incorporation of Li in carbonate minerals is still highly ambiguous. Earlier works in geological carbonate samples have shown that the Li/Ca ratio of foraminiferal calcite is not related to the temperature, whereas in brachiopods the Li/Ca ratio decreases with increasing temperature (Delaney et al., 1985; 1989). Moreover, the presence of organics, as well as vital effects of corals and shells, is presumed to influence the mechanisms controlling the incorporation of Li in calcite. To explain the controlling parameters and mechanisms, such as temperature (T), pH, calcification rate, salinity, and incorporation reactions in the carbonate lattice, well constrained laboratory experiments are required. To date, however, only a few studies have investigated the mechanisms controlling the Li/Ca ratio and the Li isotope composition of calcite under laboratory conditions. For instance, Marriott et al. (2004a) demonstrated that the ratio of Li/ Ca of calcite decreases with increasing formation temperature and decreasing salinity (Marriott et al., 2004b). However, parameters such as mineral growth rate and pH have not so far been explored. Thus the aim of the present study is to explore the mechanisms that control the Li incorporation during the growth of calcite focusing on the influence of growth rate and pH.

1.2. Mechanisms of monovalent cation incorporation in carbonate minerals

The presence of monovalent metal cations (Me^+) such as Na^+ in naturally-occurring carbonate minerals has been well documented in the literature and a few models have been developed for their position in the crystal lattice (White, 1977; 1978; Busenberg and Plummer; 1985; Yoshimura et al., 2017). We note here that in contrast to divalent cations, the incorporation of monovalent cations (Me^+) is not affected only by size difference between the trace element and the host ion (Wang and Xu, 2001; Mavromatis et al., 2018) but also by the charge imbalance that is imposed by their presence in the solid phase. Earlier studies suggested that Me^+, specially Na^+, may be present in calcite and aragonite at interstitial sites (White, 1977; 1978; Ishikawa and Ichikuni, 1984; Oomori et al., 1985; Okumura and Kitano, 1986), which would result in a positive charge excess that can be compensated by the presence of monovalent anions or anion complexes (like OH^-, HCO_3^- or Cl^-). In a similar double substitution model Busenberg and Plummer (1985) proposed the replacement of one Ca^{2+} ion with two Na^+ ions which is accompanied with structural incorporation of SO_4^{2-}. Finally, the presence of an anion vacancy for the incorporation of Na^+ and K^+ in aragonite has been suggested (White, 1977) in a model where two Ca^{2+} ions are replaced by two Na^+ ions with a CO_3^{2-} vacancy.

1.3. Partitioning coefficients

The partitioning of divalent metal cations (Me^{2+}) between $CaCO_3$ minerals and the forming aqueous phase is generally defined as

$$D_{Me^{2+}} = \frac{(c_{Me}/c_{Ca})_{calcite}}{(m_{Me^{2+}}/m_{Ca^{2+}})_{solution}} \qquad (1)$$

where C_{Me} and C_{Ca} denote the concentration of trace element and calcium in the solid phase, respectively and $m_{Me^{2+}}$ and $m_{Ca^{2+}}$ denote the aqueous concentrations of free Me^{2+} and Ca^{2+} ions, respectively. In experimental studies performed at 1 bar CO_2 and pH of ~6.2, the ratio of the molarities in Eq. (1) is commonly replaced by the ratio of total aqueous concentrations owing to the fact that free cations comprise typically more than 95% of the total concentration of the dissolved metal ion (Tesoriero and Pankow, 1996; Lakshtanov and Stipp, 2007; Mavromatis et al., 2013). The partitioning coefficient of Me^{2+} in $CaCO_3$ minerals, as defined in Eq. (1), is based on the assumption of an ideal substitution between a calcium ion with a divalent cation in the crystal lattice of the $CaCO_3$ phase. In other words the formation of a dilute ideal solid-solution is assumed. This model is further supported by spectroscopic studies (e.g. Reeder et al., 1999), which suggest that impurities in calcite have a 6-fold coordination with respect to oxygen ions, similar to that of Ca in this mineral phase. This model is also valid for large divalent cations such as Sr^{2+} and Ba^{2+} in the solid phase, although they regularly occur in 9-fold coordination in aqueous media.

The definition of a partitioning coefficient for the incorporation of monovalent cations from an aqueous phase to $CaCO_3$ minerals, however, is not straightforward, as an one-to-one substitution for Ca^{2+} cannot be considered. As such, the apparent partitioning coefficients of Me^+ in calcium carbonate minerals are commonly expressed as the ratio of total aqueous monovalent metal and Ca concentrations without any correction for the molarities of the free ions (e.g. Ishikawa and Ichikuni, 1984; Marriott et al., 2004a; 2004b). In this study, we report apparent partitioning coefficients of Me^+ into calcite as:

$$D^*_{Me^+} = \frac{(c_{Me}/c_{Ca})_{calcite}}{(m_{Me^+}/m_{Ca^{2+}})_{solution}} \qquad (2)$$

where c stands for the concentration of the metal ion in calcite, m_{Me^+} denotes the molar concentration of free Me^+ in the aqueous phase and $m_{Ca^{2+}}$ is the molar concentration of free Ca ions. This approach follows a similar nomenclature for that used in Eq. (1) for the formation of a diluted solid-solution from aqueous fluids (Tesoriero and Pankow, 1996; Prieto, 2009); we note here, that this does not imply a formation of solid-solution in the case of monovalent ions incorporation in calcite. The use of the molarity of the free ions in Eq. (2) considers the formation of aqueous complexes, a process that is significant for Ca within the pH range explored in this study.

2. METHODS

2.1. Experimental set-up

The incorporation of Li in calcite was studied at 25 °C as a function of mineral growth rate and pH of the reactive fluid. The experimental set-up is illustrated in Fig. 1 and is similar to that used earlier for pH controlled experiments

in our earlier studies (Mavromatis et al., 2015; Mavromatis et al., 2019). Initially, the reactor contained 0.5 L of a 0.3 M NaCl solution that was equilibrated with calcite at the pre-defined pH conditions in advance of the co-precipitation runs. Prior to the onset of the experiment, ~1 g of calcite seed material (Sigma-Aldrich, >99%) was introduced into the reactor, together with a Li (i.e. LiCl) bearing solution. The background electrolyte was fixed at 0.3 M NaCl. Calcite overgrowth on the seed material was induced by the simultaneous pumping of two separate solutions into the reaction vessel using a peristaltic pump, the first containing $CaCl_2$ and LiCl and the second Na_2CO_3. The concentrations of $CaCl_2$ and Na_2CO_3 in the inlet solutions were for each run equal and varied between 0.025 and 0.1 M. The increase in the concentration of the inlet solutions resulted in increasing surface normalized calcite growth rate under chemical steady-state conditions.

During the course of an experimental run, the pH of the reactive fluid remained constant, as achieved by the continuous bubbling of CO_2 and N_2 gas mixtures. For experiments at pH of ~6.3 the bubbling gas was pure CO_2, whereas at pH of ~8.1–8.4 atmospheric air was introduced in the reactor. For experiments conducted at pH > 9.0, constant pH conditions were achieved by titration of 0.5 M NaOH into the reactor vessel. Note here that in order to minimize evaporation, the gas phase was bubbled through a 0.3 M NaCl solution prior to its introduction into the reaction vessel. The inflow of the two inlet solutions in each reactor occurred at a rate of ~10 mL/day for each solution and induced an increase of the volume of the reactive fluid. Thus, every 24 h, a volume of reactive fluid, equal to the sum of the volumes of the inlet solutions added in 24 h by the peristaltic pump, was removed from the reactor so that the fluid volume in the reactor remained constant within ±4%. In this study, experiments 5_40 to 5_100 performed at increased inflow rates of ~20 mL/day for each inlet solution in order to increase the actual surface normalized calcite growth rate. In these experiments sampling of the reactive fluid was performed more than once per day. Stirring was stopped shortly prior to sampling to allow the solid material to settle. In this way solid removal was minimized and the solid:solution ratio was kept quasi-constant during the course of a run. Immediately after sampling, the fluid was filtered through a 0.2 μm Millipore cellulose acetate syringe filter and a sub-sample was acidified for further analyses of Ca, Li, and Na concentrations. Reactive fluid carbonate alkalinity was determined in a second sub-sample, whereas the fluid pH was measured in situ. At the end of the experimental runs, the fluid was separated from the solid phase via vacuum filtration using a 0.1 μm filter (Millipore, cellulose acetate). The solids were rinsed with Milli-Q water to remove adsorbed ions on the crystal surfaces and subsequently dried at 40 °C.

2.2. Analytical procedures

2.2.1. Solution characterization

Elemental concentrations of reactive fluids and digested solids were measured using a Perkin Elmer Optima 8300 DV Inductively coupled plasma optical emission spectrom-
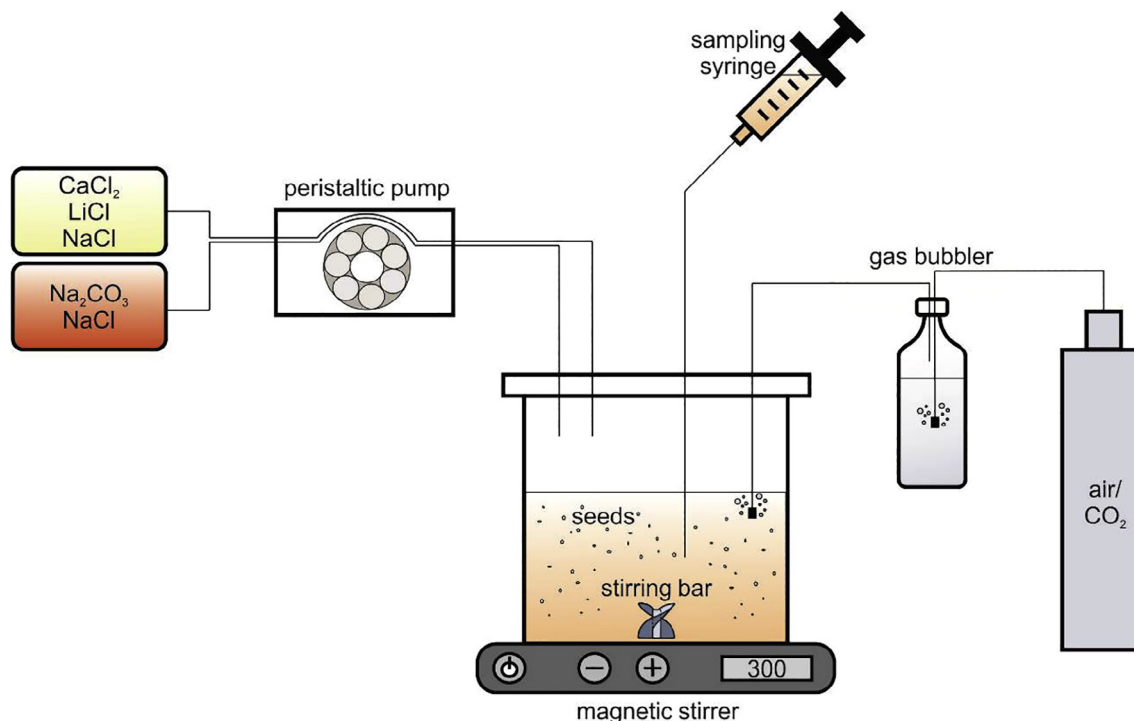
Fig. 1. Experimental set-up for the calcite growth experiments.

eter (ICP-OES) with an analytical precision of $<\pm 3$ %. The alkalinity of fluid samples was measured by standard HCl titration using an automatic Schott TitroLine alpha plus titrator with an uncertainty of $\pm 2\%$. The pH was measured using a SenTix® 945 pH gel electrode from WTW, calibrated against NIST standard buffers at pH = 4.01, 7.00 and 10.01 at 20 °C. Precision of pH measurements was ± 0.04 units and the slope of the calibration was -57 (± 1) mV per pH unit. Aqueous speciation, ion activities and saturation states (Ω) of the reactive fluids with respect to calcite were calculated using PHREEQC software together with its MINTEQ.V4 database (Parkhurst and Appelo, 1999).

2.2.2. Solid characterization

The collected solids were analyzed using an Attenuated Total Reflectance - Fourier Transform Infrared Spectrometer (ATR-FTIR; Perkin Elmer Spectrum 100) in the range of 650–4000 cm^{-1}. X-ray powder diffraction (XRD) patterns were recorded using a PANalytical X´Pert PRO diffractometer and Co-Kα-radiation (40 mA, 40 kV) from 4° to 85° at a scan speed of 0.03° min^{-1}. The mineral phases were quantified by Rietveld refinement using the PANalytical X'Pert HighScore Plus software with the PDF-2 database. Selected solids were imaged using a ZEISS DSM 982 Gemini scanning electron microscope (SEM) operating at 2 kV accelerating voltage. The specific surface area of solid samples was determined by multi-point krypton adsorption BET method (Brunauer et al., 1938) using a Quantachrome Gas Sorption system.

3. RESULTS

3.1. Mineralogy of the precipitated solids

X-ray diffraction patterns of the precipitates suggest calcite was the only mineral phase present, as did FT-IR spectra which matched the calcite reference material. SEM images showed that the precipitated solids (Fig. 2B) kept the characteristic rhombohedron-like of the seed material, consistent with the presence of calcite alone (Fig. 2A). They consisted of aggregates of rhombohedral crystals with overgrowth features on the seed surface (Fig. 2B).

3.2. Chemical composition of reactive fluids and growth rate calculation

Steady-state conditions with respect to aqueous calcium concentrations were achieved between 1000 and 3000 min depending on the applied pumping rate (Fig. 3). In contrast, Li concentrations appeared to be at steady-state conditions from the onset of the experimental runs (Fig. 3). Calcite growth rates expressed in mol m^{-2} s^{-1}, were estimated based on mass balance considerations using the number of moles of Ca introduced in the reactor per unit time and corrected for the number of moles of Ca removed over the same period of time via sampling, after reaching chemical steady-state conditions, according to the expression

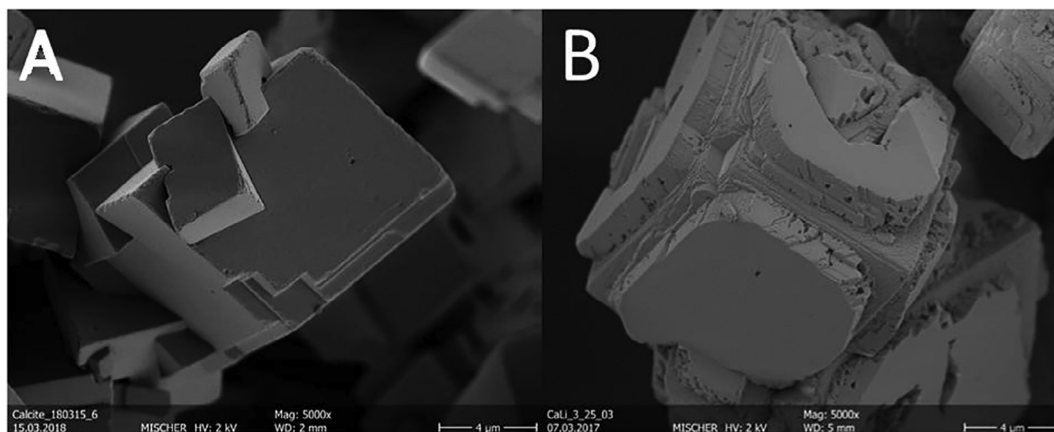$$Rate = \frac{n_{Ca(add)} - n_{Ca(rem)}}{86400} / S \tag{3}$$

Fig. 2. Scanning Electron Microphotographs of (A) calcite seeds used for the calcite growth experiments and (B) final overgrow precipitates (Experiment CaLi3-25).

where n stands for the number of moles of calcium added into the reactor and removed from the reactor within 24 h, S denotes the total calcite surface (m^2) and 86,400 stands for the number of seconds in 24 h (Mavromatis et al. 2013; 2015). Note here that growth rate estimation based on Eq. (3) is not taking into account the incorporation of traces such as Li and Na in the precipitated calcite as the respective amounts are negligible compared to Ca. The obtained overall variation in growth rates in experiments conducted herein lays within the range $-8.2 \leq \mathrm{Log}Rate \leq -7.1$ (see Table 1) and it exhibits a linear correlation with saturation degree of the reactive fluid with respect to calcite for experiments conducted under similar inlet solution inflow rates as it can be seen in electronic supplement (ESM) Fig. 1.

3.3. Lithium and sodium partitioning between calcite and solution

The apparent partitioning coefficients of Li and Na in the precipitated calcite have been calculated based on the
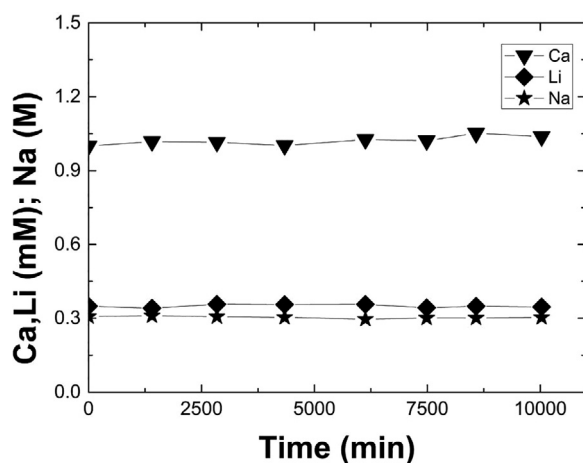

Fig. 3. Temporal evolution of Ca, Li and Na as a function of time for experimental run CaLi3_40. Analytical uncertainty is included in the symbol size.

molarities of the respective free aqueous ions after the attainment of chemical steady-state conditions using Eq. (2). Note here that no corrections applied to the Na concentrations in experiments performed at pH ~9.5 (i.e. 7_25, 7_50 and 7_100) for the amount of Na that was additionally added in the reactive fluid via NaOH titration. This is because the overall amount of Na added in a course of a run was ≤ 3 mmoles and it did not measurably increase the Na concentration of the reactive fluid (see ESM Table 1). The molarities of aqueous complexes considered in this study are shown in the ESM Table 1. Note that the concentration of Me$^+$ in the solid phase used in Eq. (2) has been corrected for the amount of seed material in the bulk precipitate. The amount of the precipitate varied between ~0.2 and ~3.0 g among the experimental runs

Obtained results for D^*_{Li} and D^*_{Na} are provided in Table 1. Overall D^*_{Li} and D^*_{Na} values range within $-4.8 \leq \mathrm{Log}D^*_{Li} \leq -2.8$ and $-5.4 \leq \mathrm{Log}D^*_{Na} \leq -2.9$, respectively. There is a notable correlation of D_{Li}^* with growth rate for experiments conducted in the pH range between 8.0 and 8.3 (Fig. 4). This correlation is also reflected in the variation of D^*_{Li} with the saturation degree of the reactive fluid with respect to calcite as it is depicted in ESM Fig. 2. The positive correlation between D^*_{Li} and $Rate$ can be described by the linear relationship

$$\mathrm{Log}D^*_{Li} = 1.331(\pm 0.116) \times \mathrm{Log}Rate + 5.966(\pm 0.880);$$
$$\mathrm{R}^2 = 0.87 \quad\quad\quad (4)$$

In similar terms Na incorporation in calcite, over the same pH range, can be described as a function of growth rate using the linear equation:

$$\mathrm{Log}D^*_{Na} = 1.413(\pm 0.202) \times \mathrm{Log}Rate + 6.039(\pm 1.527);$$
$$\mathrm{R}^2 = 0.72 \quad\quad\quad (5)$$

Furthermore, the experimental results indicate that the pH of the reactive fluid has a strong effect on the D^*_{Li} value. Indeed, as is illustrated in Fig. 5, at the lowest pH value employed in the experiments of this study of about 6.3,

Table 1
Chemical composition of Li and Ca in the reactive fluid at chemical steady-state conditions, pH, estimated growth rate and distribution coefficients of Li and Na in the forming calcite during the experimental runs calculated from both molarities of free ions and total aqueous concentrations.

Experiment	Li_{ss} (mM)	Ca_{ss} (mM)	Alkalinity (mM)	pH	Log$Rate$	LogD^*_{Li}	LogD^*_{Na}	LogD_{Li}	LogD_{Na}
2_30[*]	0.35	0.99	2.7	8.27	−8.1	−4.7	−5.5	−4.3	−5.1
2_40[*]	0.34	1.12	2.6	8.29	−8.0	−4.5	−5.5	−4.1	−5.1
2_50	0.34	0.39	3.4	8.56	−8.1	−5.1	−5.7	−4.7	−5.3
2_60[*]	0.35	1.35	2.3	8.23	−7.8	−4.5	−5.6	−4.1	−5.2
2_70[*]	0.34	1.37	2.5	8.27	−7.7	−4.5	−5.5	−4.1	−5.1
2_80[*]	0.36	1.69	2.3	8.29	−7.6	−4.1	−5.4	−3.7	−5.0
2_90	0.35	0.78	2.6	8.40	−7.6	−4.5	−5.5	−4.1	−5.1
2_100[*]	0.35	1.61	2.3	8.25	−7.5	−3.9	−4.6	−3.5	−4.2
3_25[*]	0.35	1.32	2.2	8.23	−7.9	−4.5	−5.2	−4.1	−4.8
3_30[*]	0.35	0.89	2.6	8.35	−7.9	−4.7	−5.7	−4.3	−5.3
3_40[*]	0.35	1.04	2.4	8.33	−7.8	−4.4	−5.5	−4.0	−5.1
3_50[*]	0.35	1.73	2.1	8.17	−7.6	−4.3	−4.9	−3.9	−4.5
3_60[*]	0.34	1.30	2.3	8.30	−7.5	−4.3	−5.3	−3.8	−4.9
3_70[*]	0.36	1.33	2.2	8.28	−7.4	−4.1	−5.4	−3.7	−5.0
3_80[*]	0.35	1.85	2.2	8.28	−7.4	−3.9	−4.9	−3.5	−4.5
3_100[*]	0.35	2.11	2.2	8.34	−7.3	−3.6	−5.0	−3.2	−4.6
5_40[*]	0.41	1.41	2.6	8.10	−7.5	−3.9	−4.6	−3.5	−4.2
5_50[*]	0.45	1.49	2.7	8.07	−7.4	−3.6	−4.3	−3.2	−3.9
5_60[*]	0.44	1.49	2.6	8.13	−7.3	−3.7	−4.5	−3.3	−4.1
5_70[*]	0.45	1.72	2.5	8.04	−7.3	−3.7	−4.4	−3.3	−4.0
5_80[*]	0.40	1.27	2.7	8.09	−7.2	−3.7	−4.5	−3.3	−4.1
5_90	0.50	4.55	2.2	7.87	−7.2	−3.3	−4.1	−2.9	−3.7
5_100[*]	0.40	2.22	2.3	7.99	−7.1	−3.5	−4.4	−3.1	−4.0
7_25	0.31	0.10	2.8	9.59	−8.1	−5.2	−5.7	−4.8	−5.3
7_50	0.31	0.11	2.8	9.43	−7.8	−5.0	−5.7	−4.6	−5.3
7_100	0.31	0.14	2.6	9.54	−7.5	−5.1	−5.5	−4.6	−5.2
12_60	0.24	9.27	20.9	6.29	−7.8	−3.3	−3.3	−2.9	−2.8
12_70	0.26	7.47	20.6	6.34	−7.7	−3.4	−3.5	−3.0	−3.0
12_80	0.28	12.17	21.6	6.31	−7.7	−3.4	−3.5	−2.9	−3.0
12_100	0.24	9.51	22.3	6.31	−7.6	−3.3	−3.6	−2.8	−3.1
13_60	0.24	3.17	5.7	7.41	−7.7	−3.7	−4.1	−3.2	−3.7
13_70	0.25	3.56	5.3	7.49	−7.7	−3.7	−4.1	−3.3	−3.6
13_80	0.23	3.09	6.5	7.50	−7.7	−3.6	−4.2	−3.1	−3.8
13_100	0.24	3.10	5.4	7.44	−7.7	−3.7	−4.2	−3.3	−3.7

[*] Indicates samples used in Fig. 4.

D^*_{Li} reached its highest value of $10^{-2.9}$. In contrast, at the highest pH value of about 9.5, D^*_{Li} yielded its lowest value of $10^{-4.8}$. The negative relation of D^*_{Li} with pH for experiments conducted at almost constant growth rates (i.e. $10^{-7.7\pm0.2}$ mol m^{-2} s^{-1}) can be expressed using the linear equation

$$Log D^*_{Li} = -0.57(\pm0.047) \times pH + 0.759(\pm0.366);$$
$$R^2 = 0.90; 6.3 < pH < 9.5 \qquad (6)$$

The observed dependence of the obtained $D^*_{Me^+}$ values on growth rate calculated in this study is in good agreement with the general behavior of divalent hydrophilic cations with $D_{Me^{2+}} \ll 1$ values. Those exhibit an increase in partitioning between solid and fluid with increasing growth rates (e.g., Lorens, 1981; Tesoriero and Pankow, 1996; Tang et al., 2008a; Mavromatis et al., 2013). Similarly, for the monovalent cation, Na$^+$, it has previously been shown that its incorporation in calcite is strongly affected by growth rate (Busenberg and Plummer, 1985; Mucci, 1988). Finally,

the apparent partitioning coefficients, D^*_{Li}, calculated in this study based on Eq. (4) are in good agreement with those reported previously by Marriott et al. (2004a; 2004b).

4. DISCUSSION

4.1. The role of growth rate on Li incorporation in calcite

The results of the present study suggest a strong variation of the D^*_{Li} value of about two orders of magnitude over a narrow pH range. Indeed, as depicted in Fig. 4, the D^*_{Li} values increase from $10^{-4.8}$ to $10^{-2.9}$ as calcite growth rate increases from $10^{-8.1}$ to $10^{-7.1}$ (mol m^{-2} s^{-1}). Considering that this increase in D^*_{Li} occurs within a narrow pH range of $8.0 \leq pH \leq 8.3$, and from the constant background electrolyte composition in all experimental runs (i.e. ~0.3 M NaCl) it can be reasonably deduced that under these conditions the parameter controlling the incorporation of Li in calcite is the growth rate.
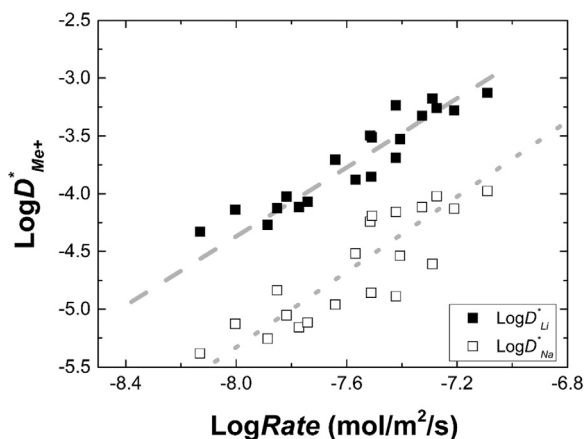
Fig. 4. Apparent partition coefficient of Li and Na between calcite and reactive fluid plotted as a function of calcite growth rate for experiments conducted in the range $8.0 \leq pH \leq 8.3$. Analytical uncertainty is included in the symbol size.
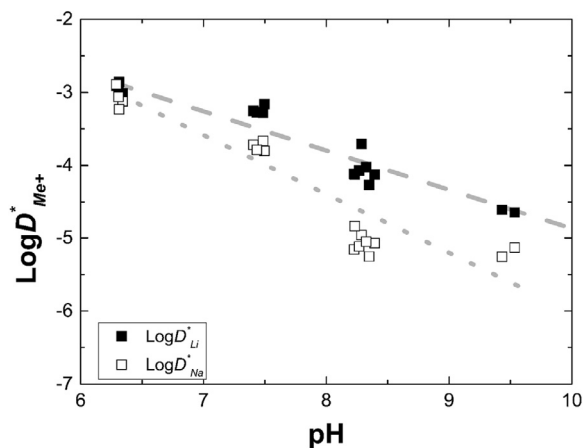

Fig. 5. Apparent partition coefficient of Li and Na between calcite and reactive fluid plotted as a function of pH for experiments conducted at similar growth rates (i.e. $10^{-7.7 \pm 0.2}$). Analytical uncertainty is included in the symbol size.

Growth rate effects on elemental partitioning during calcium carbonate mineral growth have been documented for a large number of traces/impurities. As described by Rimstidt et al. (1998), with increasing growth rate the elemental partitioning of divalent cations during their incorporation in a metal carbonate mineral phase tends towards unity. This behavior implies that at elevated growth rates elemental discrimination, as is postulated by thermodynamic considerations, is no longer valid, and the elemental ratio of trace to major ion in the precipitate approaches that of the forming fluid. Such behavior has been experimentally shown to be valid for a large number of divalent cations during calcite growth (i.e. Ba^{2+}, Cd^{2+}, Co^{2+}, Fe^{2+}, Mn^{2+}, Ni^{2+}, Sr^{2+}, Zn^{2+}; Lorens, 1981; Pingitore and Eastman, 1984, 1986; Dromgoole and Walter, 1990; Tesoriero and Pankow, 1996; Temmam et al., 2000; Lakshtanov and Stipp 2007; Tang et al.,

2008a; Mavromatis et al., 2013; 2017a; 2018). A similar behavior has been shown to be valid for anions like borate, sulphate and phosphate, where incorporation in calcite is characterized by small partitioning coefficients (Busenberg and Plummer, 1985; House, 1990; Mavromatis et al., 2015; Uchikawa et al., 2015; 2017; Wynn et al., 2018).

The impact of growth rate on Li partitioning in calcite can be explained by the growth entrapment model (GEM) developed by Watson and co-workers (Watson and Liang, 1995; Watson, 1996, 2004). This model has previously been used to describe the incorporation of divalent metal (Me^{2+}) cations in calcite. The GEM states that during rapid growth of calcite crystals, trace elements that are incompatible with the calcite structure are enriched in a surface layer of the freshly forming crystal. This implies that the partitioning coefficient of hydrophilic divalent cations, $D_{Me^{2+}} < 1$, which can form a solid-solution with calcite via the direct substitution of Me^{2+} with Ca^{2+} in the crystal lattice, would increase at elevated growth rates. Over the last decades GEM has been successfully applied to describe elemental partitioning of divalent cations between carbonate minerals and fluids (Gabitov and Watson, 2006; Gaetani and Cohen, 2006; Gabitov et al., 2008, 2012; Tang et al., 2008a; 2008b; Mavromatis et al., 2013).

In comparison to other impurities in calcite, both cations and anions, Li partitioning exhibits likely the strongest correlation to growth rate as demonstrated in Fig. 4. Indeed, with an increase of ~2 orders of magnitude in D_{Li}^* values over an increase of about one order of magnitude in growth rate, Li concentrations in calcite are likely a very sensitive indicator of mineral growth in comparison to other ions. For example, Mg exhibits an increase of only about 0.5 orders of magnitude over a two order of magnitude increase in growth rate (Mavromatis et al., 2013). As discussed above, the incorporation of monovalent cations in carbonate minerals is not occurring via direct substitution of Ca^{2+} ion in the calcite structure. In the case of Na^+ incorporation in calcite, D_{Na}^* is suggested to depend on the density of crystal surface defects (Busenberg and Plummer; 1985; Mucci, 1988), a feature that increases with precipitation rate (Teng et al., 2000). Accordingly, it is likely that the reaction mechanism controlling Li^+ incorporation in calcite is the same as that for Na^+. Okumura and Kitano (1986), reached the same conclusion, and inferred this mechanism also for K^+ and Rb^+. The similar mechanism of Li^+ and Na^+ incorporation in calcite is further supported by the very similar *rate* dependence of $D_{Me^+}^*$ (see data in Fig. 4). Indeed the slopes of D_{Li}^* and D_{Na}^* as defined in Eqs. (4) and (5), respectively, are identical within the error of estimation of apparent partitioning coefficients. The difference in the absolute $D_{Me^+}^*$ values of about one order of magnitude is likely explained by the difference in ionic radii between Li^+ and Na^+ (Okumura and Kitano, 1986). In an aqueous phase, Li^+ occurs as a 6-coordinated ion with a radius of 0.76 Å (Shannon, 1976), whereas 6-fold coordinated Na^+ is ~25% larger with an ionic radius of 1.02 Å (Shannon, 1976). As such, it can be assumed that the introduction of Me^+ ions in the calcite lattice is somewhat affected by their ionic radii.

4.2. The role of pH on Li incorporation in calcite

The findings of this study suggest that the growth rate at which calcite forms strongly controls the D_{Li}^* value. As it is depicted in Fig. 5, however, pH has also a strong control over the measured D_{Li}^* values. Indeed, for experiments conducted under similar surface normalized growth rates (i.e. $10^{-7.7\pm0.2}$ mol m^{-2} s^{-1}) D_{Li}^* exhibits a strong reduction from $10^{-3.3}$ to $10^{-5.1}$ as pH increases from ~6.3 to ~9.5. A similar pH dependence has previously been shown for B incorporation in calcite and aragonite (Mavromatis et al., 2015; Uchikawa et al., 2015). A comparison between these two elements is not straightforward, however, as aqueous speciation of B (i.e. $^{[III]}$B and $^{[IV]}$B) is strongly pH dependent, whereas aqueous Li occurs primarily as Li$^+$ independent of fluid pH. As such, the decreasing D_{Li}^* values at elevated pH conditions are likely associated with the mechanism of Li incorporation in the crystal structure and do not reflect changes in aqueous speciation. The similar incorporation behavior of Na$^+$ suggests a common mechanism responsible for the incorporation of monovalent cations in the calcite structure. The pH dependence of D_{Na}^*, however, as depicted in Fig. 5, follows a somewhat different trend as a function of pH. This difference likely stems from the formation of Na$^+$ aquo-complexes with HCO$_3^-$ and CO$_3^{2-}$ (i.e. NaHCO$_3^o$ and NaCO$_3^-$; ESM Table 1). We note here that an adsorption mechanism controlling Li$^+$ and Na$^+$ incorporation in the growing calcite cannot be completely excluded, as at elevated pH cation adsorption tends to increase due to rising electrostatic attraction (e.g. Appelo and Postma, 2007).

One of the major questions raised by the observed pH-dependent Me$^+$ partitioning in calcite is related to the mechanism of Me$^+$ incorporation in the crystal lattice. As discussed above, the presence of monovalent cations in the calcite crystal lattice is accompanied by a positive charge excess that can potentially be balanced by the presence of anions. As is illustrated in Fig. 6, D_{Li}^* in the experiments conducted in this study exhibits a positive correlation with the activity of aqueous bicarbonate ion (i.e. $a_{HCO_3^-}$). Moreover, as it is depicted in ESM Fig. 3, D_{Li}^* exhibits a positive relationship with the activity of aqueous HCO$_3^-$ bearing species (i.e. CaHCO$_3^+$, and NaHCO$_3°$) and a negative relationship with the activity of CO$_3^{2-}$ bearing species (i.e. CO$_3^{2-}$, and NaCO$_3^-$) likely due to their pH dependent distribution. The observed correlation between $a_{HCO_3^-}$ and D_{Li}^* is also controlled by the prevailing pH with an overall decrease of $a_{HCO_3^-}$ values at increasing pH, similar to the D_{Li}^* trend presented in Fig. 5. Note here that a direct comparison of the $a_{HCO_3^-}$ among experiments conducted at different pH values is not straightforward as the prevailing dissolved inorganic carbon concentration, here presented as alkalinity (Table 1), varies among runs due to the pH dependent solubility of calcite. The co-variation of $a_{HCO_3^-}$ with D_{Li}^*, however, likely suggests that HCO$_3^-$ might compensate the Li$^+$ excess through an ion coupled incorporation mechanism. Note here that recently Andersson et al. (2016) suggested on the basis of density functional theory calculations that HCO$_3^-$ is stable on the calcite surface as

an adsorbed species, even at circum-neutral pH conditions where CO$_3^{2-}$ is only a minor dissolved carbon species in the aqueous phase. The correlation observed in Fig. 6, however, does not necessarily preclude the association of Li$^+$ with HCO$_3^-$ in the crystal lattice of the final forming calcite. Indeed, Yoshimura et al. (2017) suggested using synchrotron X-ray spectroscopy that Na$^+$ in calcite and aragonite is accompanied by a CO$_3^{2-}$ vacancy. This vacancy, however, does not exclude the presence of HCO$_3^-$ surface species during Me$^+$ uptake on the growing surface and points towards a re-arrangement of this ion during Me$^+$ incorporation.

4.3. Implications for the Li content of natural calcite

The results of the present study clearly indicate that growth rate plays a major role in the Li content of calcite. We note here that a direct comparison with marine-grown carbonates of either biogenic or abiotic origin may not be straightforward and the proposed growth rate effect as numerically described by Eq. (4) may not be directly applicable. This is because in the experiments conducted herein reactive fluids do not contain major ions present in seawater such as Mg^{2+} and SO$_4^{2-}$ that readily incorporate in calcite (Mucci and Morse, 1983; Busenberg and Plummer, 1985; Mavromatis et al., 2017a; 2017b). The different size of such impurities compared to the structural units of calcite (i.e. Ca^{2+} and CO$_3^{2-}$) may alter the crystallographic structure of the mineral and thus promote increasing or decreasing incorporation of small ions such as Li$^+$. Overall, the partitioning of Li in natural calcites can potentially be used as a tool for estimating the formation rate, likely together with ratios of other elements such as Mg/Ca.

Another significant finding of this work that has direct implications for the interpretation of Li/Ca ratios in natural calcites is the strong negative correlation with pH. A dependence of Li content with dissolved inorganic carbon in
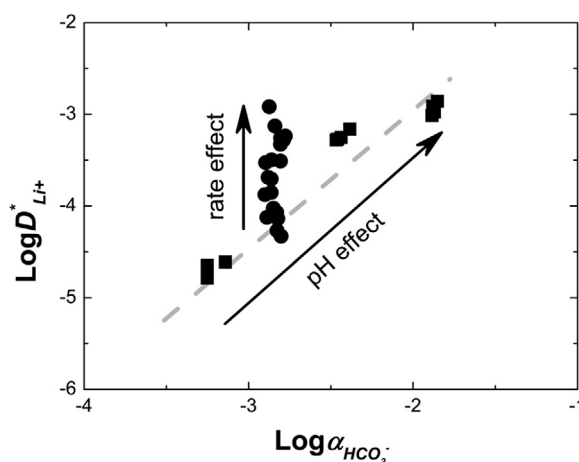

Fig. 6. Apparent partition coefficient of Li in calcite and reactive fluid plotted as a function of activity of aqueous bicarbonate ion. Experiments at pH 8.1–8.4 where growth rate has been increased are represented by circles. Analytical uncertainty is included in the symbol size.

calcite has previously been shown to exist in marine-derived carbonates such as foraminifera (Dawber and Tripati, 2012; Vigier et al., 2015). Although such dependence, or likely the availability of aqueous HCO_3^-, may be valid for marine carbonates, the highly buffered pH of oceanic waters which has stayed quasi-constant over the last 100 ka (Foster, 2008) together with the biological controls that may affect the composition of the hard parts of calcifiers such as foraminifera, suggest that the observed pH-dependence (Fig. 5) cannot directly be applied to marine carbonates. In the case of continental carbonate deposits, e.g. travertine formation, where significant pH variations occur, Li/Ca ratios may provide insights on formation conditions.

Finally, our results suggest a positive correlation between the apparent partitioning coefficients of Li and Na according to the equation:

$$LogD_{Li}^* = 0.707 \ (\pm0.054) \times LogD_{Na}^* - 0.563 \ (\pm0.242);$$
$$R^2 = 0.84 \tag{7}$$

This relation is valid for all the experimental runs independently of calcite growth rate. Measured Li/Na ratios in natural calcites can thus be used to estimate the Na^+ concentration in the precipitating fluid from Eq. (7) if its Li^+ concentration is known or can be reasonably estimated (and vice versa for Na^+). Considering that for natural samples, as for example seawater, the Me^+/Ca concentration ratios are commonly used instead of those for activities, we have plotted in Fig. 7B the partitioning coefficient relationship using total Li and Na aqueous concentrations using the notation D_{Me}. This relationship can be expressed as:

$$LogD_{Li} = 0.699 \ (\pm0.052) \times LogD_{Na} - 0.602 \ (\pm0.229);$$
$$R^2 = 0.85 \tag{8}$$

and it exhibits a slope similar to that of Eq. (7). Note here that the application of Eq. (8) in natural waters like seawater is not straightforward. This is because it has been calculated for calcites precipitated from a solution with a background electrolyte of ~0.3 M NaCl that does not contain other major ions like Mg^{2+} and SO_4^{2-}. The latter ions are abundant at high concentrations in seawater and well known to affect carbonate mineral formation (e.g. Mucci and Morse, 1983; Busenberg and Plummer, 1985)

5. CONCLUSIONS

The experimental work performed in this study documents that the incorporation of Li in calcite during its growth is affected by at least two parameters, the growth rate and the pH. The observed increase of Li incorporation in the growing calcite can be well explained by the surface entrapment approach that was previously developed by Watson and co-workers (Watson, 1996; 2004; Watson and Liang, 1995). In the case of monovalent cations such as Li^+ and Na^+, entrapment is associated with the presence of defects on crystal surface. The occurrence of such defects is expected to increase at elevated calcite growth rates, similar to the apparent Li partitioning coefficients measured herein. As such, the experimental results imply that Li/Ca ratios in natural calcites can be used as a tool for the estimation of mineral growth rates. Moreover, the similar behavior of sodium and lithium during their incorporation into calcite indicates that the introduction of monovalent cations in calcite is controlled by the same mechanism though absolute partitioning values are affected by ionic radii. The linear correlation of the apparent partitioning coefficients of Li and Na in the forming calcite is independent of growth rate effects, thus Li/Na ratios in natural calcites may be used as a novel tool for reconstructing Na or Li concentration of the aqueous fluids from which calcite formed.

The experimental results suggest that incorporation of monovalent cations in the calcite crystal lattice may be associated with the presence of HCO_3^-. Whether the bicarbonate ion is introduced in the crystal lattice or not cannot be concluded from the present study and has to be assessed in forthcoming high resolution spectroscopic studies.
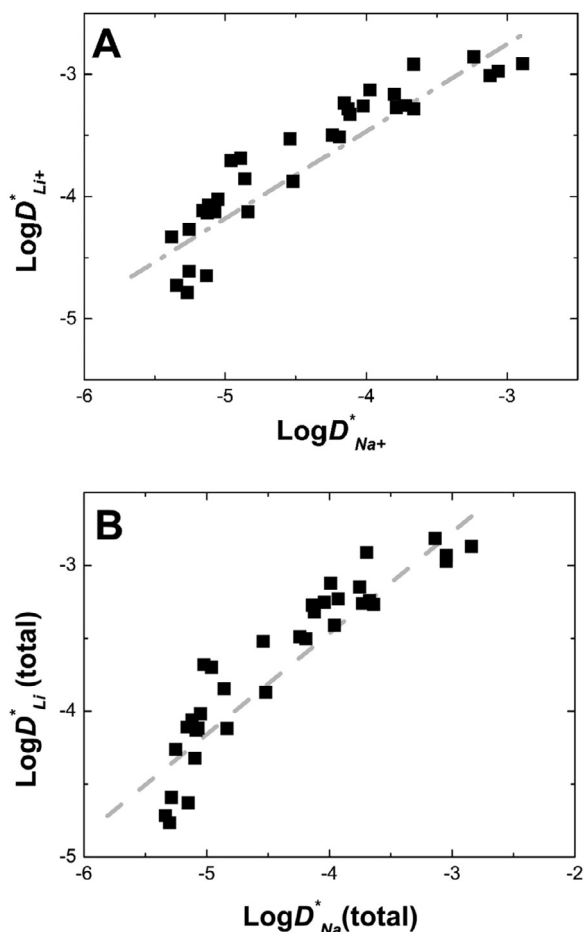

Fig. 7. Apparent partition coefficient of Li vs Na. in calcite (A) calculated based on the abundance of free ions in the reactive fluid and (B) calculated based on the total concentrations of Li and Na in the reactive fluid. Analytical uncertainty is included in the symbol size.

APPENDIX A. SUPPLEMENTARY MATERIAL

Supplementary data to this article can be found online at https://doi.org/10.1016/j.gca.2018.12.040.

REFERENCES

Andersson M. P., Rodriguez-Blanco J. D. and Stipp S. L. S. (2016) Is bicarbonate stable in and on the calcite surface?. *Geochim. Cosmochim. Acta* **176** 198–205.

Appelo C. A. J. and Postma D. (2007) Geochemistry, Groundwater and Pollution, 2nd ed. A.A. Balkema Publishers, Leiden.

Boettcher M. E. (1998) Manganese(II) partitioning during experimental precipitation of rhodochrosite-calcite solid solutions from aqueous solutions. *Mar. Chem.* **62**, 287–297.

Brunauer S., Emmet P. H. and Teller E. (1938) Adsorption of gases in multimolecular layers. *J. Am. Chem. Soc.* **60**, 309–319.

Bryan S. P. and Marchitto T. M. (2008) Mg/Ca-temperature proxy in benthic foraminifera: New calibrations from the Florida Straits and a hypothesis regarding Mg/Li. *Paleoceanography* **23** (PA2220).

Burton K. W. and Vigier N. (2011) Lithium isotopes as tracers in marine and terrestrial environment. In *Handbook of Environmental Isotope Geochemistry* (ed. M. Baskaran).

Busenberg E. and Plummer L. N. (1985) Kinetic and thermodynamic factors controlling the distribution of SO_4^{2-} and Na^+ in calcites and selected aragonites. *Geochim. Cosmochim. Acta* **49**, 713–725.

Chan L. H., Edmond J. M., Thompson G. and Gillis K. (1992) Lithium isotopic composition of submarine basalts: implications for the lithium cycle in the oceans. *Earth Planet. Sci. Lett.* **108**, 151–160.

Dawber C. F. and Tripati A. K. (2012) Relationships between bottom water carbonate saturation and element/Ca ratios in coretop samples of the benthic foraminifera Oridorsalis umbonatus. *Biogeosciences* **9**, 3029–3045.

Delaney M. L., Bé A. W. H. and Boyle E. A. (1985) Li, Sr, Mg, and Na in foraminiferal calcite shells from laboratory culture, sediment traps, and sediment cores. *Geochim. Cosmochim. Acta* **49**, 1327–1341.

Delaney M. L., Popp B. N., Lepzlter C. G. and Anderson T. F. (1989) Lithium-to-calcium ratios in modern, cenozoic, and paleozoic articulate braciiiopod shells. *Paleoceanography* **4**, 681–691.

Dietzel M., Gussone N. and Eisenhauer A. (2004) Co-precipitation of Sr^{2+} and Ba^{2+} with aragonite by membrane diffusion of CO_2 between 10 and 50 °C. *Chem. Geol.* **203**, 139–151.

Dietzel M. and Usdowski E. (1996) Coprecipitation of Ni^{2+}, Co^{2+}, and Mn^{2+} with galena and covellite, and of Sr^{2+} with calcite during crystallization via diffusion of H_2S and CO_2 through

polyethylene at 20 degrees C: Power law and Nernst law control of trace element partitioning. *Chem. Geol.* **131**, 55–65.

Dromgoole E. L. and Walter L. M. (1990) Iron and manganese incorporation into calcite - effects of growth-kinetics, temperature and solution chemistry. *Chem. Geol.* **81**, 311–336.

Foster G. L. (2008) Seawater pH, PCO_2 and CO_3^2 variations in the Caribbean Sea over the last 130 kyr: A boron isotope and B/Ca study of planktic forminifera. *Earth Planet. Sci. Lett.* **271**, 254–266.

Gabitov R. I., Gaetani G. A., Watson E. B., Cohen A. L. and Ehrlich H. L. (2008) Experimental determination of growth rate effect on U^{6+} and Mg^{2+} partitioning between aragonite and fluid at elevated U^{6+} concentration. *Geochim. Cosmochim. Acta* **72**, 4058–4068.

Gabitov R. I., Rollion-Bard C., Tripati A. and Sadekov A. (2014a) In situ study of boron partitioning between calcite and fluid at different crystal growth rates. *Geochim. Cosmochim. Acta* **137**, 81–92.

Gabitov R. I., Sadekov A. and Leinweber A. (2014b) Crystal growth rate effect on Mg/Ca and Sr/Ca partitioning between calcite and fluid: An in situ approach. *Chem. Geol.* **367**, 70–82.

Gabitov R. I. and Watson E. B. (2006) Partitioning of strontium between calcite and fluid. *Geochem. Geophys. Geosyst.* **7**.

Gabitov R. I., Watson E. B. and Sadekov A. (2012) Oxygen isotope fractionation between calcite and fluid as a function of growth rate and temperature: An in situ study. *Chem. Geol.* **306**, 92–102.

Gaetani G. A. and Cohen A. L. (2006) Element partitioning during precipitation of aragonite from seawater: A framework for understanding paleoproxies. *Geochim. Cosmochim. Acta* **70**, 4617–4634.

Hall J. M. and Chan L. H. (2004) Li/Ca in multiple species of benthic and planktonic foraminifera: Thermocline, latitudinal, and glacial–interglacial variation. *Geochim. Cosmochim. Acta* **68**, 529–545.

House W. A. (1990) The prediction of phosphate co-precipitation with calcite in fresh-waters. *Water Res.* **24**, 1017–1023.

Huh Y., Chan L. H. and Edmond J. M. (2001) Lithium isotopes as a probe of weathering processes: Orinoco River. *Earth Planet. Sci. Lett.* **194**, 189–199.

Ishikawa M. and Ichikuni M. (1984) Uptake of sodium and potassium by calcite. *Chem. Geol.* **42**, 137–146.

Lakshtanov L. Z. and Stipp S. L. S. (2004) Experimental study of europium(III) co-precipitation with calcite. *Geochim. Cosmochim. Acta* **68**, 819–827.

Lakshtanov L. Z. and Stipp S. L. S. (2007) Experimental study of nickel(II) interaction with calcite: Adsorption and co-precipitation. *Geochim. Cosmochim. Acta* **71**, 3686–3697.

Lear C. H., Mawbey E. M. and Rosenthal Y. (2010) Cenozoic benthic foraminiferal Mg/Ca and Li/Ca records: Toward unlocking temperatures and saturation states. *Paleoceanography* **25**, PA4215.

Lear C. H. and Rosenthal Y. (2006) Benthic foraminiferal Li/Ca: Insights into Cenozoic seawater carbonate saturation state. *Geology* **34**, 985–988.

Lorens R. B. (1981) Sr, Cd, Mn and Co distribution coefficients in calcite as a function of calcite precipitation rate. *Geochim. Cosmochim. Acta* **45**, 553–561.

Marriott C. S., Henderson G. M., Belshaw N. S. and Tudhope A. W. (2004a) Temperature dependence of δ^7Li, $\delta^{44}Ca$ and Li/Ca during growth of calcium carbonate. *Earth Planet. Sci. Lett.* **222**, 615–624.

Marriott C. S., Henderson G. M., Crompton R., Staubwasser M. and Shaw S. (2004b) Effect of mineralogy, salinity, and temperature on Li/Ca and Li isotope composition of calcium carbonate. *Chem. Geol.* **212**, 5–15.

Mavromatis V., Gautier Q., Bosc O. and Schott J. (2013) Kinetics of Mg partition and Mg stable isotope fractionation during its incorporation in calcite. *Geochim. Cosmochim. Acta* **114**, 188–203.

Mavromatis V., Goetschl K. E., Grengg C., Konrad F., Purgstaller B. and Dietzel M. (2018) Barium partitioning in calcite and aragonite as a function of growth rate. *Geochim. Cosmochim. Acta* **237**, 65–78.

Mavromatis V., Gonzàlez G. A., Dietzel M. and Schott J. (2019) Zinc isotope fractionation during the inorganic precipitation of calcite - Towards a new pH proxy Geochim. *Cosmochim. Acta* **244**, 99–112.

Mavromatis V., Immenhauser A., Buhl D., Purgstaller B., Baldermann A. and Dietzel M. (2017a) Effect of organic ligands on Mg partitioning and Mg isotope fractionation during low-temperature precipitation of calcite in the absence of growth rate effects. *Geochim. Cosmochim. Acta* **207**, 139–153.

Mavromatis V., Montouillout V., Noireaux J., Gaillardet J. and Schott J. (2015) Characterization of boron incorporation and speciation in calcite and aragonite from co-precipitation experiments under controlled pH, temperature and precipitation rate. *Geochim. Cosmochim. Acta* **150**, 299–313.

Mavromatis V., Purgstaller B., Dietzel M., Buhl D., Immenhauser A. and Schott J. (2017b) Impact of amorphous precursor phases on magnesium isotope signatures of Mg-calcite. *Earth Planet. Sci. Lett.* **464**, 227–236.

Misra S. and Froelich P. N. (2012) Lithium Isotope History of Cenozoic Seawater: Changes in Silicate Weathering and Reverse Weathering. *Science* **335**, 818–824.

Mucci A. (1988) Manganese uptake during calcite precipitation from seawater - conditions leading to the formation of a pseudokutnahorite. *Geochim. Cosmochim. Acta* **52**, 1859–1868.

Mucci A. and Morse J. W. (1983) The incorporation of Mg^{2+} and Sr^{2+} into calcite overgrowths; influences of growth rate and solution composition. *Geochim. Cosmochim. Acta* **47**, 217–233.

Négrel P., Millot R., Brenot A. and Bertin C. (2010) Lithium isotopes as tracers of groundwater circulation in a peat land. *Chem. Geol.* **276**, 119–127.

Okumura M. and Kitano Y. (1986) Co-precipitation of alkali metal ions with calcium carbonate. *Geochim. Cosmochim. Acta* **50**, 49–58.

Oomori T., Nakasone M., Kanechima K. and Kitano Y. (1985) Incorporation of sodium into calcium carbonate and proto-dolomite. *Bull. Coll. Sci.* **39**, 51–56.

Parkhurst D. L. and Appelo C. A. J. (1999) User's guide to PHREEQC (Version 2)—a computer program for speciation, bath-reaction, one-dimensional transport, and inverse geo-chemical calculations. *Water-Resources Investigations Report 99–4259*. USGS, Denver CO, USA.

Pingitore, Jr., N. E. and Eastman M. P. (1984) The experimental partitioning of Ba^{2+} into calcite. *Chem. Geol.* **45**, 113–120.

Pingitore, Jr., N. E. and Eastman M. P. (1986) The co-precipitation of Sr^{2+} with calcite at 25 °C and 1 atm. *Geochim. Cosmochim. Acta* **50**, 2195–2203.

Prieto M. (2009) Thermodynamics of solid solution – aqueous solution systems. *Rev. Mineral. Geochem.* **70**, 47–85.

Purgstaller B., Konrad F., Dietzel M., Immenhauser A. and Mavromatis V. (2017) Control of Mg^{2+}/Ca^{2+} activity ratio on the formation of crystalline carbonate minerals via an amorphous precursor. *Cryst. Growth Des.* **17**, 1069–1078.

Purgstaller B., Mavromatis V., Immenhauser A. and Dietzel M. (2016) Transformation of Mg-bearing amorphous calcium carbonate to Mg-calcite – In situ monitoring. *Geochim. Cosmochim. Acta* **174**, 180–195.

Reeder R. J., Lamble G. M. and Northrup P. A. (1999) XAFS study of the coordination and local relaxation around Co^{2+}, Zn^{2+}, Pb^{2+}, and Ba^{2+} trace elements. *Am. Miner.* **84**, 1049–1060.

Rimstidt J. D., Balog A. and Webb J. (1998) Distribution of trace elements between carbonate minerals and aqueous solutions. *Geochim. Cosmochim. Acta* **62**, 1851–1863.

Shannon R. T. (1976) Revised effective ionic radii and systematic studies of interatomic distances in halides and chalcogenides. *Acta Crystallogr. Sect. A* **32**, 751–767.

Tang J., Dietzel M., Boehm F., Koehler S. J. and Eisenhauer A. (2008a) Sr^{2+}/Ca^{2+} and $^{44}Ca/^{40}Ca$ fractionation during inorganic calcite formation: II Ca isotopes. *Geochim. Cosmochim. Acta* **72**, 3733–3745.

Tang J., Koehler S. J. and Dietzel M. (2008b) Sr^{2+}/Ca^{2+} and $^{44}Ca/^{40}Ca$ fractionation during inorganic calcite formation: I. Sr incorporation. *Geochim. Cosmochim. Acta* **72**, 3718–3732.

Temmam M., Paquette J. and Vali H. (2000) Mn and Zn incorporation into calcite as a function of chloride aqueous concentration. *Geochim. Cosmochim. Acta* **64**, 2417–2430.

Teng H. H., Dove P. M. and DeYoreo J. J. (2000) Kinetics of calcite growth; surface processes and relationships to macroscopic rate laws. *Geochim. Cosmochim. Acta* **64**, 2255–2266.

Tesoriero A. J. and Pankow J. F. (1996) Solid solution partitioning of Sr^{2+}, Ba^{2+}, and Cd^{2+} to calcite. *Geochim. Cosmochim. Acta* **60**, 1053–1063.

Uchikawa J., Penman D. E., Zachos J. C. and Zeebe R. E. (2015) Experimental evidence for kinetic effects on B/Ca in synthetic calcite: Implications for potential $B(OH)_4-$ and $B(OH)_3$ incorporation. *Geochim. Cosmochim. Acta* **150**, 171–191.

Vigier N., Rollion-Bard C., Levenson Y. and Erez J. (2015) Lithium isotopes in foraminifera shells as a novel proxy for the ocean dissolved inorganic carbon (DIC). *C. R. Geosci.* **347**, 43–51.

Voigt M., Mavromatis V. and Oelkers E. H. (2017) The experimental determination of REE partition coefficients in the water-calcite system. *Chem. Geol.* **462**, 30–43.

Wang Y. F. and Xu H. F. (2001) Prediction of trace metal partitioning between minerals and aqueous solutions: A linear free energy correlation approach. *Geochim. Cosmochim. Acta* **65**, 1529–1543.

Watson E. B. (1996) Surface enrichment and trace-element uptaking during crystal growth. *Geochim. Cosmochim. Acta* **60**, 5013–5020.

Watson E. B. (2004) A conceptual model for near-surface kinetic controls on the trace-element and stable isotope composition of abiogenic calcite crystals. *Geochim. Cosmochim. Acta* **68**, 1473–1488.

Watson E. B. and Liang Y. (1995) A simple model for sector zoning in slowly grown crystals: implications for growth rate and lattice diffusion, with emphasis on accessory minerals in crustal rocks. *Am. Miner.* **80**, 1179–1187.

White A. F. (1977) Sodium and potassium coprecipitation in aragonite. *Geochim. Cosmochim. Acta* **41**, 613–625.

White A. F. (1978) Sodium coprecipitation in calcite and dolomite. *Chem. Geol.* **23**, 65–72.

Wynn P. M., Fairchild I. J., Borsato A., Spötl C., Hartland A., Baker A., Frisia S. and Baldini J. U. L. (2018) Sulphate partitioning into calcite: Experimental verification of pH control and application to seasonality in speleothems. *Geochim. Cosmochim. Acta* **226**, 69–83.

Yoshimura T., Tamenori Y., Suzuki A., Kawahata H., Iwasaki N., Hasegawa H., Nguyen L. T., Kuroyanagi A., Yamazaki T., Kuroda J. and Ohkouchi N. (2017) Altervalent substitution of sodium for calcium in biogenic calcite and aragonite. *Geochim. Cosmochim. Acta* **202**, 21–38.

Associate editor: Robert H. Byrne

Update

Geochimica et Cosmochimica Acta

Corrigendum

Corrigendum to "Effect of growth rate and pH on lithium incorporation in calcite" [Geochim. Cosmochim. Acta 248 (2019) 14–24]

In the original article, Table 1, data reported in columns $LogD_{Li}^*$ and $LogD_{Na}^*$ are incorrect. This correction does not affect Eq. (7) and does not change the conclusions of the original article. The authors would like to apologize for any inconvenience that this oversight may have caused.

Table 1
Chemical composition of Li and Ca in the reactive fluid at chemical steady-state conditions, pH, estimated growth rate and distribution coefficients of Li and Na in the forming calcite during the experimental runs calculated from both molarities of free ions and total aqueous concentrations.

Experiment	Li_{ss} (mM)	Ca_{ss} (mM)	Alkalinity (mM)	pH	$LogRate$	$LogD_{Li}^*$	$LogD_{Na}^*$	$LogD_{Li}$	$LogD_{Na}$
2_30*	0.35	0.99	2.7	8.27	−8.1	−4.3	−5.4	−4.3	−5.1
2_40*	0.34	1.12	2.6	8.29	−8.0	−4.1	−5.1	−4.1	−5.1
2_50	0.34	0.39	3.4	8.56	−8.1	−4.7	−5.3	−4.7	−5.3
2_60*	0.35	1.35	2.3	8.23	−7.8	−4.1	−5.2	−4.1	−5.2
2_70*	0.34	1.37	2.5	8.27	−7.7	−4.1	−5.1	−4.1	−5.1
2_80*	0.36	1.69	2.3	8.29	−7.6	−3.7	−5.0	−3.7	−5.0
2_90	0.35	0.78	2.6	8.40	−7.6	−4.1	−5.1	−4.1	−5.1
2_100*	0.35	1.61	2.3	8.25	−7.5	−3.5	−4.2	−3.5	−4.2
3_25*	0.35	1.32	2.2	8.23	−7.9	−4.1	−4.8	−4.1	−4.8
3_30*	0.35	0.89	2.6	8.35	−7.9	−4.3	−5.3	−4.3	−5.3
3_40*	0.35	1.04	2.4	8.33	−7.8	−4.0	−5.1	−4.0	−5.1
3_50*	0.35	1.73	2.1	8.17	−7.6	−3.9	−4.5	−3.9	−4.5
3_60*	0.34	1.30	2.3	8.30	−7.5	−3.9	−4.9	−3.8	−4.9
3_70*	0.36	1.33	2.2	8.28	−7.4	−3.7	−4.9	−3.7	−5.0
3_80*	0.35	1.85	2.2	8.28	−7.4	−3.5	−4.5	−3.5	−4.5
3_100*	0.35	2.11	2.2	8.34	−7.3	−3.2	−4.6	−3.2	−4.6
5_40*	0.41	1.41	2.6	8.10	−7.5	−3.5	−4.2	−3.5	−4.2
5_50*	0.45	1.49	2.7	8.07	−7.4	−3.2	−4.2	−3.2	−3.9
5_60*	0.44	1.49	2.6	8.13	−7.3	−3.3	−4.1	−3.3	−4.1
5_70*	0.45	1.72	2.5	8.04	−7.3	−3.3	−4.0	−3.3	−4.0
5_80*	0.40	1.27	2.7	8.09	−7.2	−3.3	−4.1	−3.3	−4.1
5_90	0.50	4.55	2.2	7.87	−7.2	−2.9	−3.7	−2.9	−3.7
5_100*	0.40	2.22	2.3	7.99	−7.1	−3.1	−4.0	−3.1	−4.0
7_25	0.31	0.10	2.8	9.59	−8.1	−4.8	−5.3	−4.8	−5.3
7_50	0.31	0.11	2.8	9.43	−7.8	−4.6	−5.3	−4.6	−5.3
7_100	0.31	0.14	2.6	9.54	−7.5	−4.7	−5.1	−4.6	−5.2
12_60	0.24	9.27	20.9	6.29	−7.8	−2.9	−2.9	−2.9	−2.8
12_70	0.26	7.47	20.6	6.34	−7.7	−3.0	−3.1	−3.0	−3.0
12_80	0.28	12.17	21.6	6.31	−7.7	−3.0	−3.1	−2.9	−3.0
12_100	0.24	9.51	22.3	6.31	−7.6	−2.9	−3.2	−2.8	−3.1
13_60	0.24	3.17	5.7	7.41	−7.7	−3.3	−3.7	−3.2	−3.7
13_70	0.25	3.56	5.3	7.49	−7.7	−3.3	−3.7	−3.3	−3.6
13_80	0.23	3.09	6.5	7.50	−7.7	−3.2	−3.8	−3.1	−3.8
13_100	0.24	3.10	5.4	7.44	−7.7	−3.3	−3.8	−3.3	−3.7

* Indicates samples used in Fig. 4.

A. Füger   Institute of Applied Geosciences, Graz University of Technology,
Rechbauerstrasse 12, 8010 Graz, Austria
JR-AquaConSol GmbH, Steyrergasse 21, 8010 Graz, Austria

F. Konrad   Institute of Applied Geosciences, Graz University of Technology,
Rechbauerstrasse 12, 8010 Graz, Austria
Omya GmbH, Gersheim Straße 1-2, 9722 Gummern, Austria

A. Leis   JR-AquaConSol GmbH, Steyrergasse 21, 8010 Graz, Austria

M. Dietzel   Institute of Applied Geosciences, Graz University of Technology,
Rechbauerstrasse 12, 8010 Graz, Austria

V. Mavromatis   Institute of Applied Geosciences, Graz University of Technology,
Rechbauerstrasse 12, 8010 Graz, Austria
Géosciences Environnement Toulouse (GET), CNRS, UMR 5563,
Observatoire Midi-Pyrénées, 14 Avenue Edouard Belin, 31400
Toulouse, France